Bioavailable fractions drive variations in riverine dissolved organic nitrogen along land-use gradients

Yan Ding [a, b], Yaning Yang [a], Ting Pan [a], Yuecheng She [a], Chang Liu [a], Juan Zhao [a], Xiaowei Liu [c], Qingbo Yu [a], Fengyu Zan (✉) [a]

[a] *School of Ecology and Environment, Anhui Normal University, Wuhu 241002, China*

[b] *Collaborative Innovation Center of Recovery and Reconstruction of Degraded Ecosystem in Wanjiang Basin Co-founded by Anhui Province and Ministry of Education, School of Ecology and Environment, Anhui Normal University, Wuhu 241002, China*

[c] *School of Biology, Food, and Environment, Hefei University, Hefei 230601, China*

✉ Corresponding author.

E-mail address: zanfengyu@126.com (Fengyu Zan)

Full postal address: School of Ecology and Environment, Anhui Normal University, No. 189 Jiuhua South Road, Wuhu City 241002, China

Tel: +86-0553-5910198

Text S1. The electrodialysis pretreatment method

The volume of the compact electrodialysis reactor is 200 ml (length×width×height =10 cm×2 cm×10 cm), which included one sample pool and two salt solution chambers (Fig. T1). The electrode material of the electrodialysis reactor is platinum wire, and 0.5 mol/L sodium chloride solution is injected into the salt solution chamber. The selected anionic membrane was AMI-7001S1 and the cationic membrane was CIM-7000S1, which purchased from Membranes International Inc. (USA). The effective membrane area was 64 cm^2 for both membranes. The membrane thickness ranged from 0.425 to 0.475 mm. The total exchange capacity was 1.2–1.4 meq/g for the anion exchange membrane and 1.5–1.7 meq/g for the cation exchange membrane. The permselectivity was approximately 90% and 94% for the anion and cation exchange membranes, respectively. Both membranes exhibited high mechanical strength (> 80 psi), thermal stability up to 90 °C, and chemical stability within a pH range of 1–10.

Electrodialysis pretreatment was conducted at a constant voltage of 30 V for 40 min, followed by the determination of dissolved inorganic nitrogen (DIN). Prior to each run, membranes were rinsed with ultrapure water and conditioned in 0.5 mol/L NaCl solution. Samples were pre-filtered through 0.45 μm membranes to minimize membrane fouling, and the reactor was rinsed thoroughly between runs. The removal efficiency of DIN ranged from 87% to 98%, with a mean value of 92.5%, indicating effective elimination of inorganic nitrogen species. Meanwhile, the loss of dissolved organic carbon (DOC) was minimal, ranging from 0.78% to 11.94% (mean: 5.65%), suggesting limited impact on organic constituents (Fig. T2). These results demonstrate

that electrodialysis provides a reliable and selective pretreatment method for DON analysis, achieving efficient DIN removal while preserving the majority of organic matter. The concentration of DON in electrodialysis solution can be acquired directly by measuring TDN.

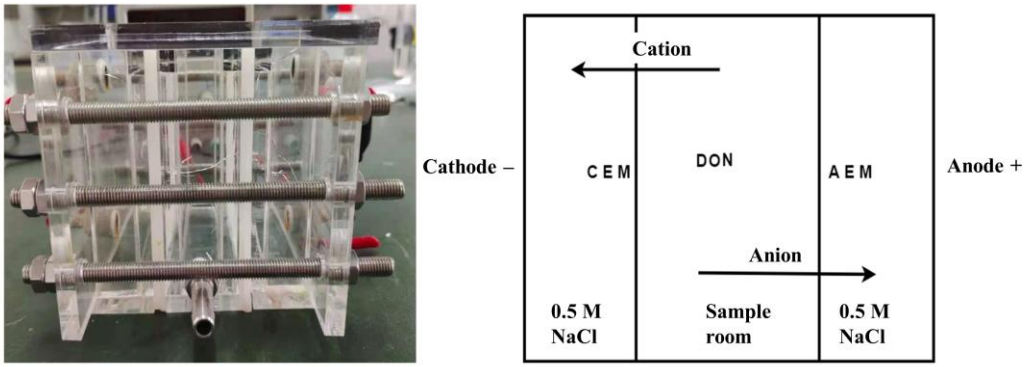

Fig. T1. Physical diagram and structure diagram of electrodialysis device

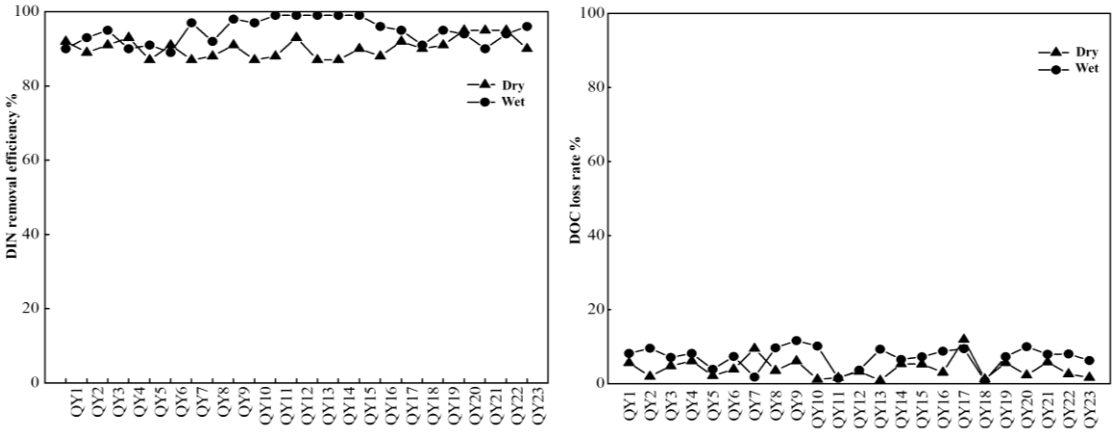

Fig. T2. DIN removal efficiency and DOC loss rate (%) after electrodialysis

Text S2. The determination process of the amino acid in DON

The amino acid components of DON in water samples were determined by pre-column derivatization high-performance liquid chromatography (HPLC) using o-phthalaldehyde (OPA). In the presence of 3-mercaptopropionic acid (3-MPA), OPA reacts with amino acids through the following reaction:

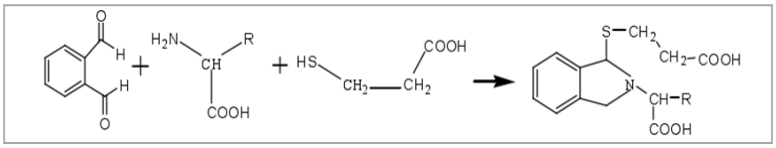

Firstly, a 0.1 g/L OPA–0.4% 3-MPA derivatization solution was prepared in 0.5 M borate buffer (pH 9.9). Briefly, 13.4 mg of ortho-phthaldialdehyde (OPA) was dissolved in 25 mL methanol, and 20 mL of the resulting OPA solution was transferred to a 100 mL volumetric flask. Subsequently, 80 μL of 3-mercaptopropionic acid (3-MPA) was added, and the solution was diluted to volume with pH 9.90 ± 0.05 borate buffer. The reagent was protected from light for >90 min to minimize background interference and stored at 4°C (stable for 9 days). Secondly, the mobile phase was prepared with component A and B. Component A contained 0.05 mol/L sodium acetate (NaAc) adjusted to pH 7.2 with 1% acetic acid (HAc), supplemented with 1.5% (v/v) tetrahydrofuran (THF). Component B was prepared with 0.1 mol/L NaAc (pH 7.2 adjusted with 1% HAc) mixed with methanol and acetonitrile at a volume ratio of 46:10:44 (NaAc: methanol: acetonitrile). The two components were then thoroughly combined, filtered through 0.45 μm membranes, and degassed by ultrasonication to stabilize baselines. Thirdly, the standard solutions (2 mg/L) were serially diluted to generate a concentration gradient (1, 5, 10, 20, 50 μg/L) and stored at 4°C until analysis.

DFAA was determined as follows: A 200 μL aliquot of OPA-3-MPA reagent was added to 500 μL of standard or sample solution. After 9 min of derivatization, 1 μL of the mixture was injected into

the HPLC system for analysis. A pretreatment protocol was conducted before DTAA was determined. 1) 150 μL of DON filtrate is transferred into a glass test vial, followed by the addition of 10 μL of 20 mg/L ascorbic acid to prevent oxidation of amino acids by nitrate ions. 2) The mixture is evaporated to dryness under a nitrogen stream, after which the glass test vial is placed into a microwave digestion vessel. 3) 700 μL of acid hydrolysis mixture (10% trifluoroacetic acid, 0.1% phenol, and high-purity HCl) was added. The vessel was purged with nitrogen, vacuum-sealed, and subjected to acid vapor hydrolysis at 156°C for 30 min. 4) After cooling, residual acid was removed under a nitrogen stream. The sample was redissolved in 600 μL of borate buffer (pH 10.00 ± 0.05). DTAA quantification of the sample is performed using HPLC like DFAA.

Text S3. The correlation of $SUVA_{254}$, $SUVA_{260}$, A_{253}/A_{203}, E_2/E_3, E_3/E_4, and E_2/E_4 with DOM properties.

1. $SUVA_{254}$ and $SUVA_{260}$, calculated as 100 times the absorbance at 254 nm or 260 nm divided by DOC concentration, serve as robust indicators of DOM aromaticity and hydrophobicity, with higher values typically reflecting greater contributions from terrestrial humic substances and more condensed aromatic structures (Li et al., 2020). According to Matilainen et al. (2011), when $SUVA_{254} > 4$, the DOM is predominantly composed of hydrophobic components, whereas when $SUVA_{254} < 3$, DOM mainly consists of hydrophilic substances.
2. The A_{253}/A_{203} ratio offers information about structural features of DOM molecules, where elevated values suggest increased aromatic ring substitution. Higher ratio values correlate with increased abundance and diversity of carbonyl, carboxyl, hydroxyl, and ester functional groups on aromatic rings. Conversely, lower ratios suggest predominantly aliphatic chain substituents on the aromatic structures (Li et al., 2014).
3. The E_2/E_3 ratio (A_{254}/A_{365}) exhibits an inverse relationship with molecular weight, serving as a sensitive indicator for distinguishing between high molecular weight humic materials and lower molecular weight components (Reyes et al., 2016). When $E_2/E_3 < 3.5$, it mainly reflects the absorption characteristics of larger organic molecules such as humic acid. When $E_2/E_3 > 3.5$, it mainly reflects the absorption characteristics of smaller organic molecules, such as fulvic acid (Ran et al., 2022).
4. E_3/E_4 (A_{300}/A_{400}) ratios provide complementary information about the humification state DOM, with higher values generally indicating less humified (Xi et al., 2018).
5. E_2/E_4 (A_{254}/A_{436}) ratios in the range 4–11 is indicative of terrestrial DOM, and 11–30 is indicative of DOM derived mostly from microbial sources. The smaller the E_2/E_4 value, the greater the degree of condensation of organic molecules.

Matilainen, A., Gjessing, E. T., Lahtinen, T., Hed, L., Bhatnagar, A., Sillanpää, M., 2011. An overview of the methods used in the characterisation of natural organic matter (NOM) in relation to drinking water treatment. Chemosphere 83(11), 1431–1442.

Li, M., Kong, F., Li, Y., He, W., Liu, W., Yang, C., Yang, B., 2020. Ecological indication based on source, content, and structure characteristics of dissolved organic matter in surface sediment from Dagu River estuary, China. Environ. Sci. Pollut. Res. 27(36), 45499–45512.

Li, Y., Wang, S., Zhang, L., Zhang, G., 2014. Composition and spectroscopic characteristics of dissolved organic matter extracted from the sediment of Erhai Lake in China. J. Soils Sediments 14(9), 1599–1611.

Reyes, T. G., Crisosto, J. M., 2016. Characterization of Dissolved Organic Matter in River Water by Conventional Methods and Direct Sample Analysis-Time of Flight-Mass Spectrometry. J. Chem. 2016, 1–11.

Xi, M., Zi, Y., Wang, Q., Guo, Y., Huang, Y., 2018. Assessment of the content, structure, and source of soil dissolved organic matter in the coastal wetlands of Jiaozhou Bay, China. Phys. Chem. Earth 103, 35–44.

Ran, S., He, T., Zhou, X., Yin, D., 2022. Effects of fulvic acid and humic acid from different sources on Hg methylation in soil and accumulation in rice. J. Environ. Sci. 119, 93–105.

Text S4. The correlation of FI, BIX, HIX, Fn(280), Fn(355), and β/α with DOM/DON properties.

1. FI is used to characterize the terrestrial versus biological sources of fulvic acid-like fluorescent substances in DOM. When FI > 1.9, it indicates that the DOM in water primarily originates from endogenous metabolic byproducts of microbial decomposition. Conversely, when FI < 1.4, it suggests that the main source of DOM is terrestrial in origin. For values between 1.4 < FI < 1.9, the DOM in water is influenced by both endogenous and terrestrial sources (Mcknight et al., 2001).
2. BIX reflects the relative contribution of recently produced autochthonous DOM, with BIX < 0.6, the fluorescent substances originate from terrestrial sources. For values between 0.6 < BIX < 0.8, biological sources are considered to make a minor contribution to the fluorescent components. When 0.8 < BIX < 1, the substances exhibit relatively strong autochthonous characteristics. At BIX > 1.0, the fluorescence demonstrates pronounced autochthonous features, indicating the fluorescent materials predominantly derive from biological activities (Huguet et al., 2009).
3. HIX quantifies the degree of DOM humification, where high values (> 10) are characteristic of highly processed, aromatic-rich terrestrial DOM, and low values (< 4) represent less humified, microbially derived material (Xi et al., 2018).
4. Fn(280) and Fn(355) help distinguish between protein-like and humic-like components respectively, with elevated Fn(280) values indicating the presence of labile, proteinaceous DOM from biological sources, and increased Fn(355) values reflecting humic substances derived from terrestrial inputs or aged organic matter (Jin et al., 2020).

5. The β/α ratio provides information about DOM lability, where higher values (> 1.0) are associated with recently produced, biologically labile organic matter, and lower values (< 0.6) suggest more refractory, processed DOM (Chaves et al., 2020).

McKnight, D. M., Boyer, E. W., Westerhoff, P. K., Doran, P. T., Kulbe, T., Andersen, D. T., 2001. Spectrofluorometric characterization of dissolved organic matter for indication of precursor organic material and aromaticity. Limnol. Oceanogr. 46(1), 38–48.

Xi, M., Zi, Y., Wang, Q., Guo, Y., Huang, Y., 2018. Assessment of the content, structure, and source of soil dissolved organic matter in the coastal wetlands of Jiaozhou Bay, China. Phys. Chem. Earth 103, 35–44.

Jin, M. Y., Oh, H. J., Shin, K. H., Jang, M. H., Kim, H. W., Choi, B., Chang, K. H., 2020. The response of dissolved organic matter during monsoon and post-monsoon periods in the regulated river for sustainable water supply. Sustainability 12(13), 5310.

Chaves, R. C., Figueredo, C. C., Boechat, I. G., de Oliveira, J. T. M., Gücker, B., 2020. Fluorescence indices of dissolved organic matter as early warning signals of fish farming impacts in a large tropical reservoir. Ecol. Indic. 115, 106389.

Table S1. Description of sampling points within a 1-km upstream catchment

Sample sites	Latitude	Longitude	River reach	Forest %	farmland %	Built up %	Distance (m)
QY1	30°51'35"	118°28'17"	Upstream	**37.38%**	36.34%	26.28%	0
QY2	30°54'26"	118°29'24"	Upstream	**23.75%**	48.79%	27.46%	8324
QY3	30°56'46"	118°29'08"	Upstream	**10.96%**	61.08%	27.96%	14549
QY4	30°59'35"	118°28'41"	Upstream	**34.62%**	35.36%	30.03%	20005
QY5	31°3'22"	118°30'34"	Midstream	0.12%	**95.98%**	3.90%	28223
QY6	31°4'09"	118°32'07"	Midstream	0.11%	**99.37%**	0.52%	32154
QY7	31°6'38"	118°33'01"	Midstream	2.37%	**96.82%**	0.81%	38223
QY8	31°8'7"	118°33'22"	Midstream	0.16%	**96.19%**	3.65%	42039
QY9	31°09'05"	118°33'32"	Midstream	0.00%	**59.37%**	40.63%	44798
QY10	31°09'11"	118°31'25"	Midstream	0.00%	**98.13%**	1.87%	48248
QY11	31°10'32"	118°30'44"	Midstream	0.07%	**94.54%**	5.39%	51227
QY12	31°11'34"	118°29'13"	Midstream	0.02%	**88.59%**	11.39%	54495
QY13	31°13'03"	118°29'32"	Midstream	0.51%	**88.13%**	11.36%	57048
QY14	31°14'22"	118°29'31"	Midstream	0.00%	**96.43%**	3.57%	59650
QY15	31°15'51"	118°28'24"	Midstream	0.71%	**93.62%**	5.67%	62832
QY16	31°16'04"	118°28'36"	Midstream	0.00%	**95.91%**	4.09%	64334
QY17	31°18'38"	118°28'29"	Midstream	0.00%	**94.65%**	5.35%	67262
QY18	31°18'49"	118°28'28"	Downstream	0.00%	81.07%	**18.93%**	70034
QY19	31°19'47"	118°25'38"	Downstream	0.04%	71.20%	**28.76%**	74372
QY20	31°19'23"	118°24'31"	Downstream	0.00%	38.94%	**61.06%**	76891
QY21	31°19'41"	118°25'16"	Downstream	0.00%	32.42%	**67.58%**	78669
QY22	31°19'12"	118°22'26"	Downstream	0.00%	3.31%	**96.69%**	81929
QY23	31°19'33"	118°21'42"	Downstream	0.00%	1.08%	**98.92%**	83277

Note: Built up at upstream is scattered villages.

Table S2. Sampling point field parameters

Sites	Depth (m)		Water temperature (℃)		pH		DO (mg/L)		ORP (mV)		Conductivity (μS/cm)	
	D	W	D	W	D	W	D	W	D	W	D	W
QY1	1.5	6	5.1	25.1	8.07	7.55	15.5	8.23	115	202	190	113
QY2	2	6.5	5.8	26.2	8.05	7.69	15	8	113	241	184	110
QY3	5	6	6.8	29	7.98	7.38	15.4	7	110	188	180	124
QY4	5	6	9.5	28.9	8.1	7.3	15	6	115	178	175	136
QY5	5	7	11.6	28.4	8.45	7.97	11.7	6.5	105	220	170	270
QY6	1.5	6.5	7.4	27.6	8.35	7.71	15.8	9.08	112	197	186	227
QY7	1.5	6	7.4	27.6	8.48	7.73	17	9.23	110	195	188	218
QY8	3	10	7.4	27.7	8.1	7.75	20	9.8	105	198	201	216
QY9	2.5	7	6	27.3	8.2	7.77	11.7	10.77	158	211	201	218
QY10	3.5	8	5.4	27.3	7.65	7.7	14.1	9.6	152	211	201	208
QY11	3.3	7	5.8	27.2	7.9	7.69	13.9	10.55	146	206	205	169.8
QY12	5	6.9	5.8	27.1	7.85	7.71	13.1	11.31	152	202	203	229
QY13	3.2	7.7	6.2	27.3	8.35	7.65	13.4	11.31	153	214	202	204
QY14	4.2	10	6.5	27.1	8.25	7.66	13.1	6.75	180	214	204	209
QY15	3.5	7.3	5	27.3	7.67	7.67	14	7.73	130	216	228	204
QY16	2	7	5.7	27.4	7.87	7.69	13.5	7.22	132	210	248	201
QY17	6	6.5	6.5	27.4	7.62	7.72	13	9.2	152	210	226	200
QY18	4	7.1	6.2	26.7	7.45	7.81	13.8	7.69	130	202	248	305
QY19	3.5	8.5	5.6	26.6	7.33	7.84	14	7.89	140	208	220	297
QY20	3.2	8	7.9	26.4	7.44	7.78	12	7.12	142	199	262	302
QY21	3.2	6.5	8.4	26.1	7.22	7.82	14.1	11.68	160	208	377	301
QY22	6.6	8.9	7.9	26.3	7.75	7.82	15	10.21	185	202	420	301
QY23	6	10.8	7.6	26.9	7.34	7.77	20	10.43	187	203	423	212

Note: the D was the dry season, and the W represented as the wet season.

Table S3. The analytical methods of chemical properties

Index	Analytical methods
TN、TDN	Alkaline potassium persulfate oxidation process
TP、TDP	Ammonium molybdate spectrophotometry
DOC	High-temperature (~680 °C) combustion catalytic oxidation method on a TOC analyzer (TOC-V CPN, Shimadzu, Japan).
NO_3^--N	UV spectrophotometry method
NH_4^+-N、NO_2^--N	GMA33xx series gas phase molecular absorption spectrometer method
COD_{cr}	Permanganate oxidation method
Chl-a	Acetone extraction spectrophotometry
Urea	Diacetylmonoxime spectrophotometry

Table S4. The gradient of mobile phase

Time/min	Mobile phase A/%	Mobile phase B/%	Flow rate（mL/min）
0	100	0	0.45
5	90	10	0.45
14	40	60	0.45
18	0	100	0.45
20	0	100	0.45
25	100	0	0.45

Table S5. The retention time of amino acids

Amino acids type	Retention Time (min)	Recovery rate (%)	Standard deviation (%)
Asp	3.812	90.1	1.8
Glu	5.267	92.8	1.5
Ser	10.988	88.9	2.6
His	12.363	93.6	0.9
Gly	13.103	89.2	2.3
Thr	13.463	93.5	1.4
Arg	14.04	103.4	1.7
Ala	14.991	96.3	2.9
Tyr	16.465	93.4	2.7
Val	17.736	101.7	1.9
Met	17.954	89.5	1.8
Phe	18.808	93.2	2.5
Ile	19.029	102.6	2.1
Leu	21.288	87.7	2.3

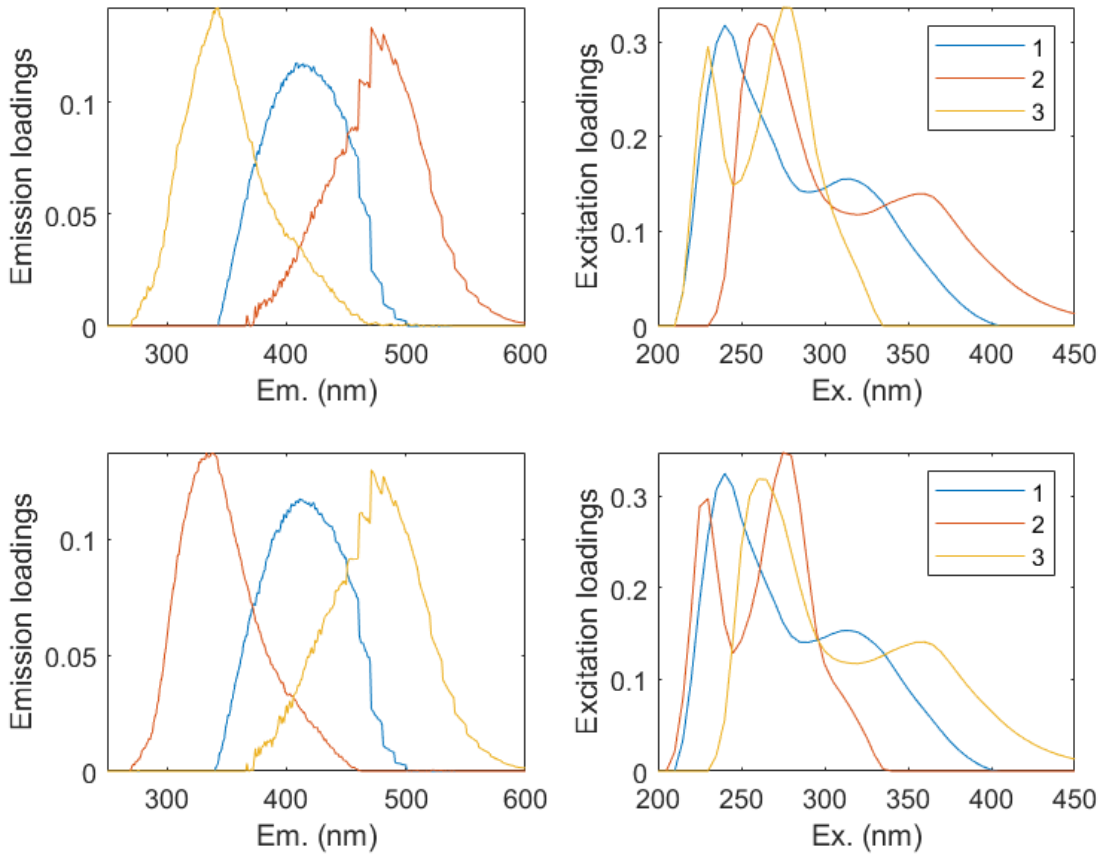

Fig. S1 Split-half validation of three components

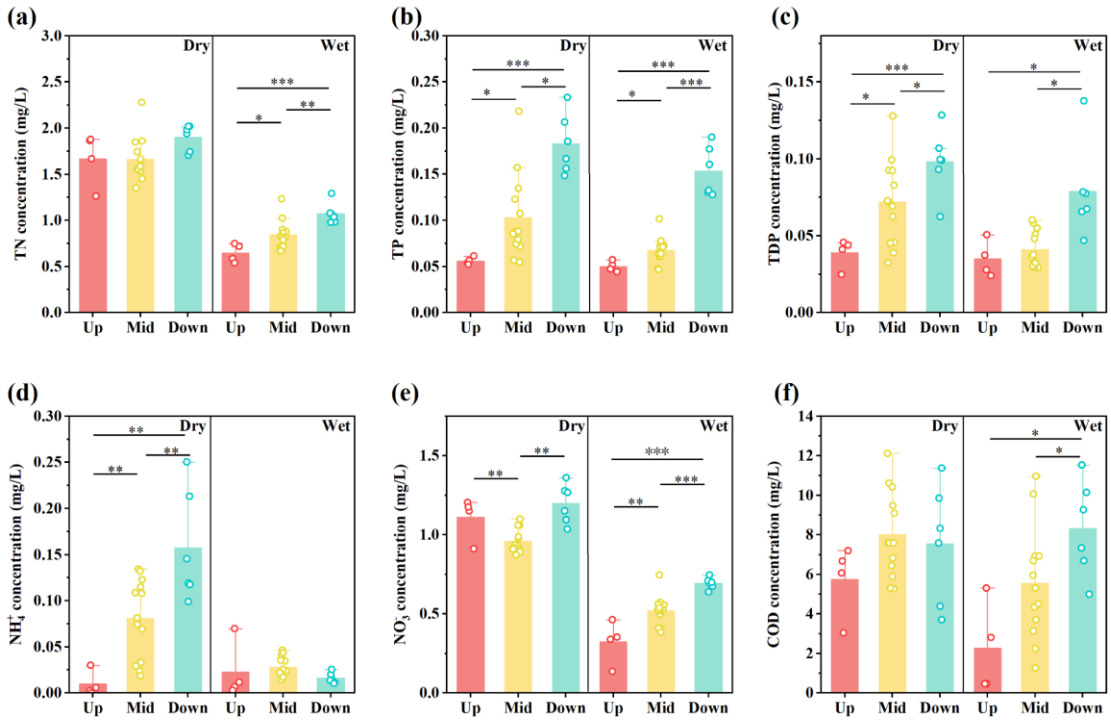

Fig. S2. Concentration variations of (a) TN, (b) TP, (c) TDP, (d) dissolved NH_4^+, (e) dissolved NO_3^-, and (f) COD in the upstream, midstream, and downstream reaches during the dry and wet seasons.

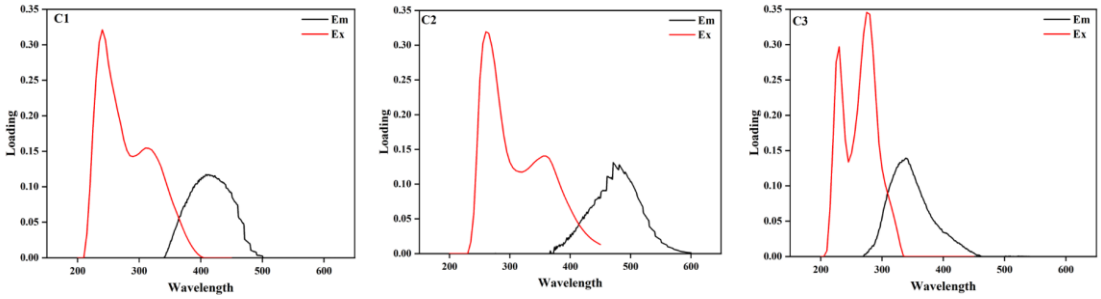

Fig. S3. The corresponding component loading plots of the three components (C1, C2, and C3) using EEM-PARAFAC analysis.

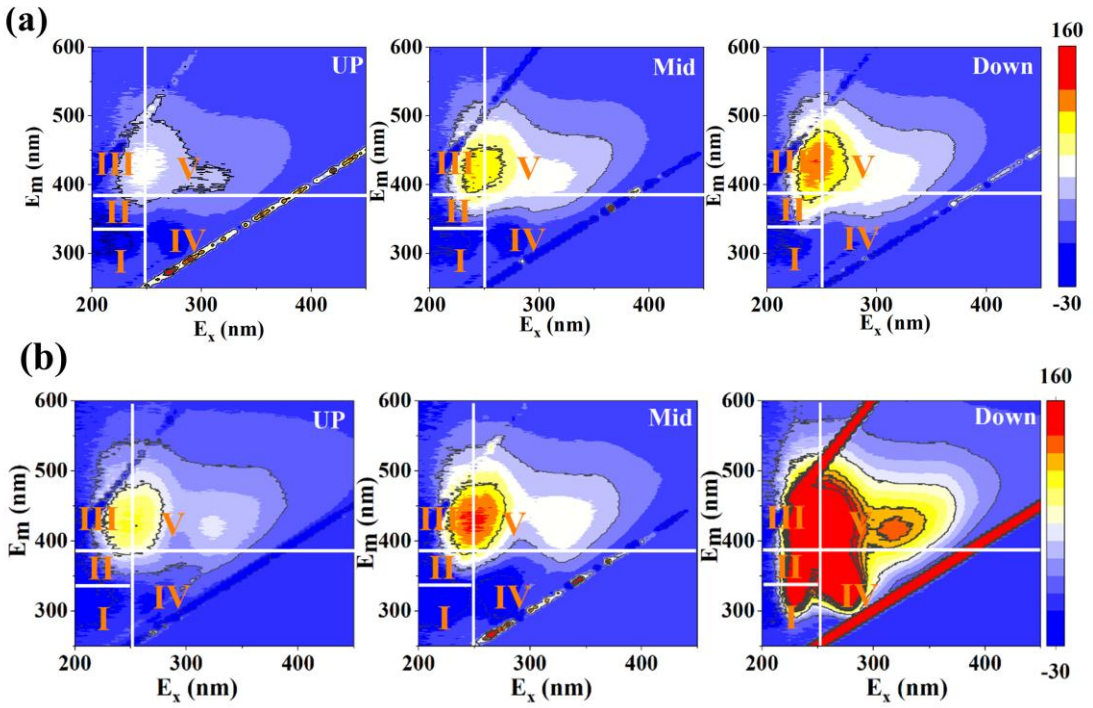

Fig. S4. Representative EEMs for upstream (QY3), midstream (QY11), and downstream (QY20) sampling sites during dry (up) and wet (down) season.

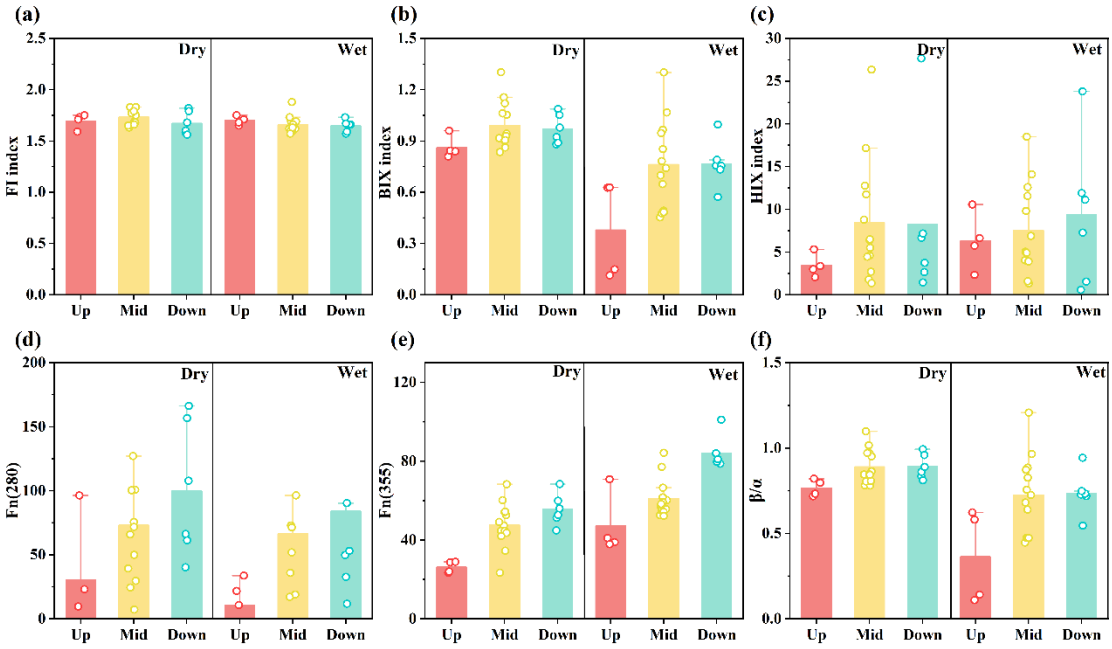

Fig. S5. Variations of (a) FI, (b) BIX, (c) HIX, (d) Fn(280), (e) Fn(355), and (f) β/α in the up-, mid-, and downstream reaches during the dry and wet seasons.

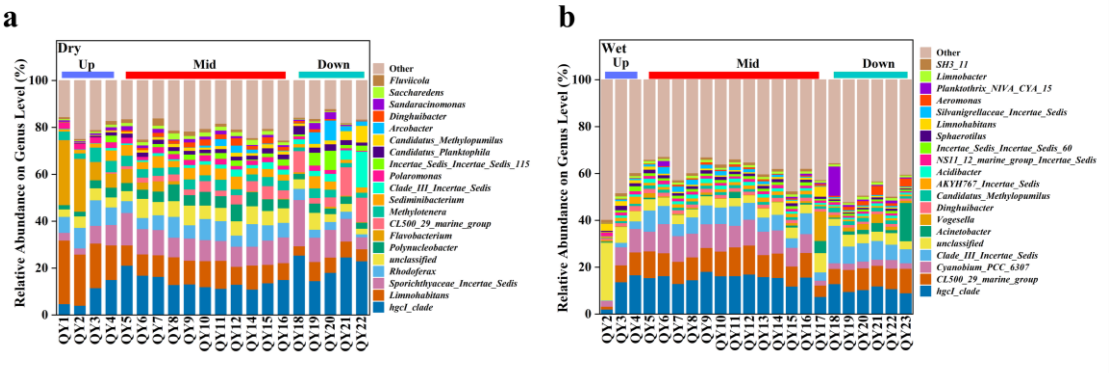

Fig. S6. Relative abundance of microbial communities at the genus level across sampling sites during dry season (a) and wet season (b)

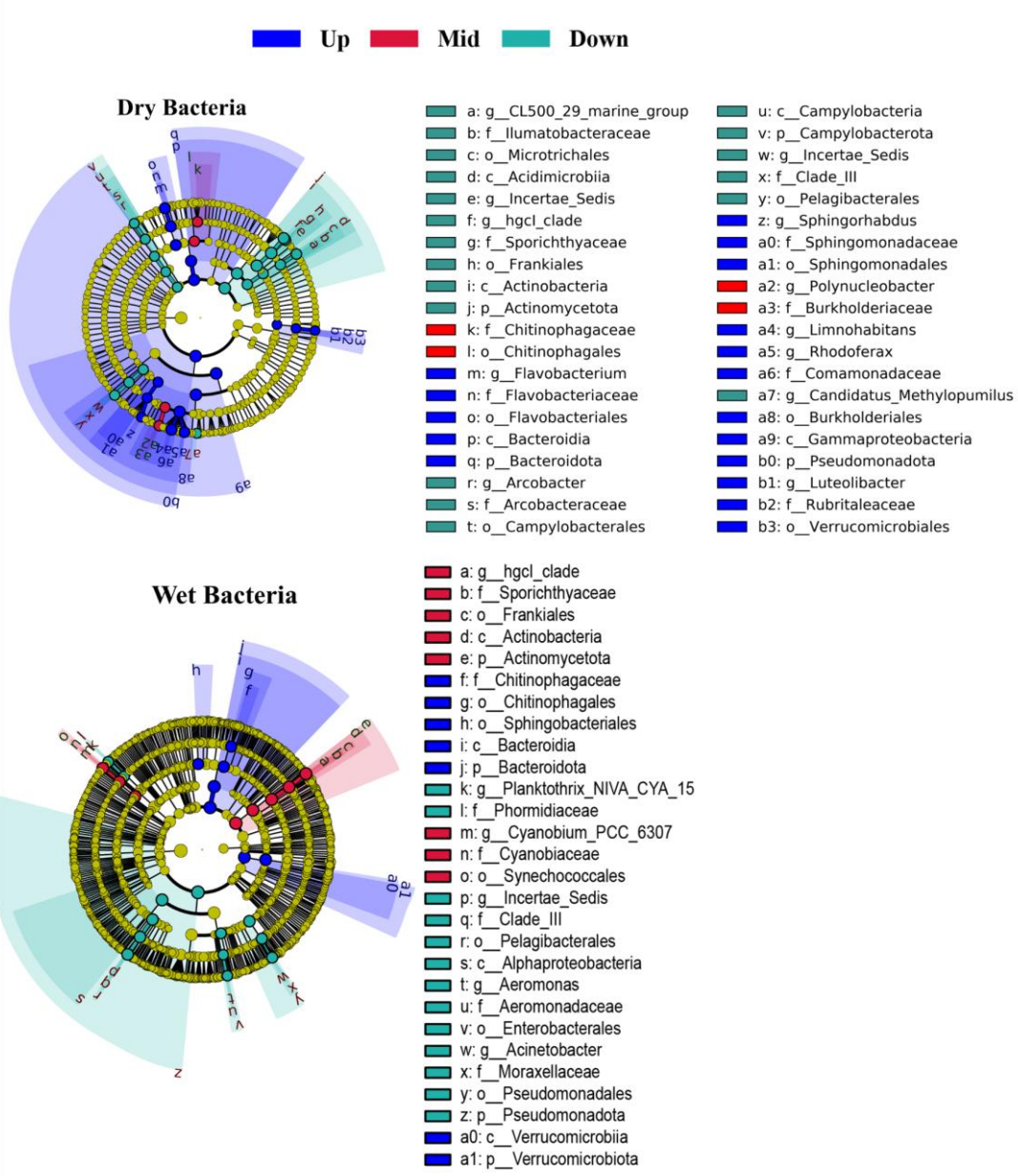

Fig. S7. Lefse analysis showing differences in bacterial communities among the three river reaches during the dry and the wet season ($p < 0.05$, LDA score > 4). Circles represent phylogenetic levels from domain to genus inside out, and differences are represented in the color of the most abundant class.

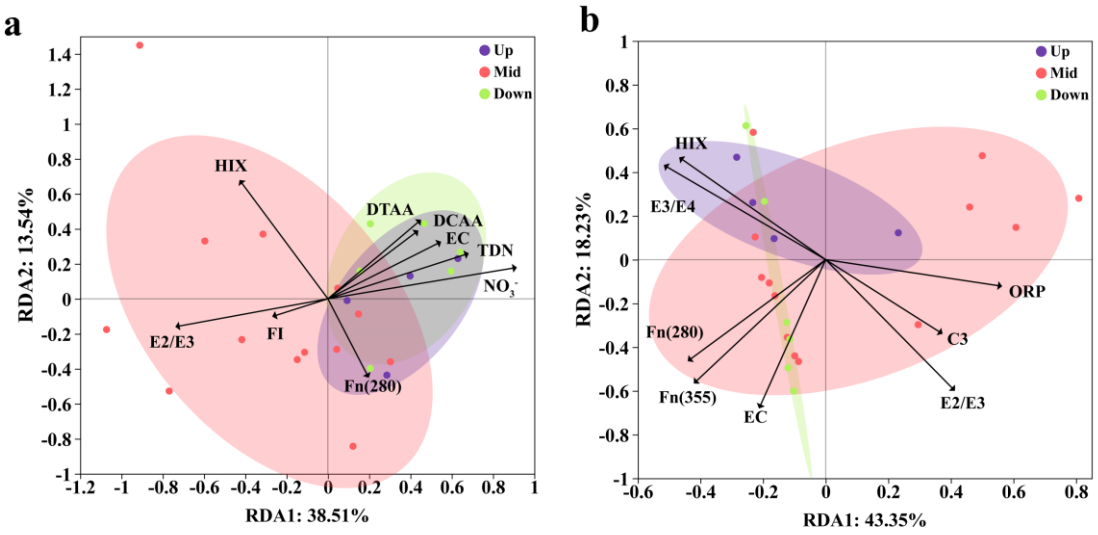

Fig. S8. RDA based on phytoplankton phylum-level abundance and environmental chemical parameters (envfit test, $p < 0.05$) during the (a) dry and (b) wet seasons.

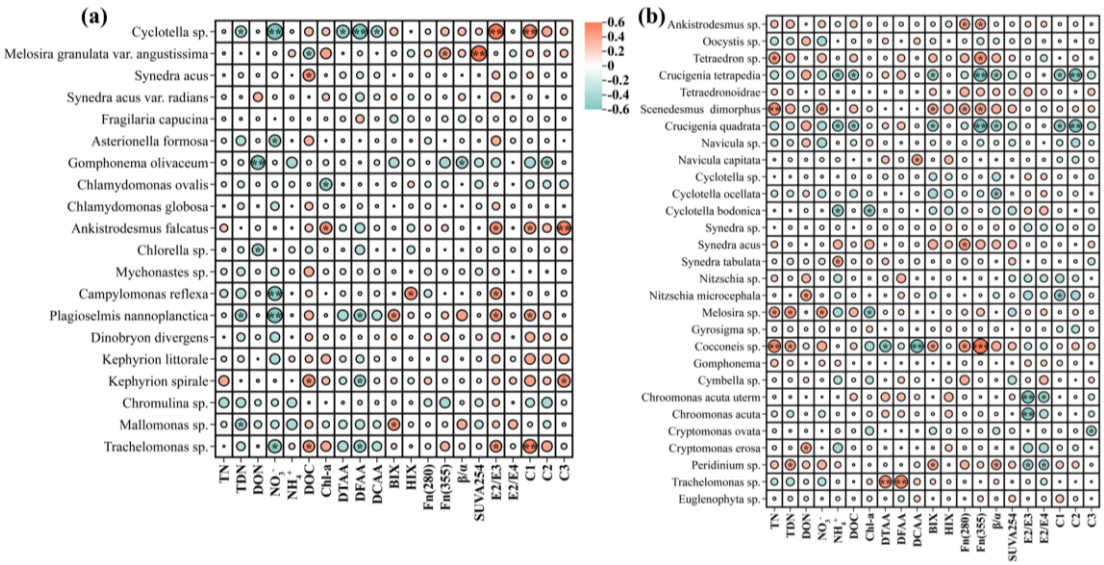

Fig. S9. Spearman correlation between nitrogen related parameters and phytoplankton abundance at species levels during (a) dry and (b) wet season.

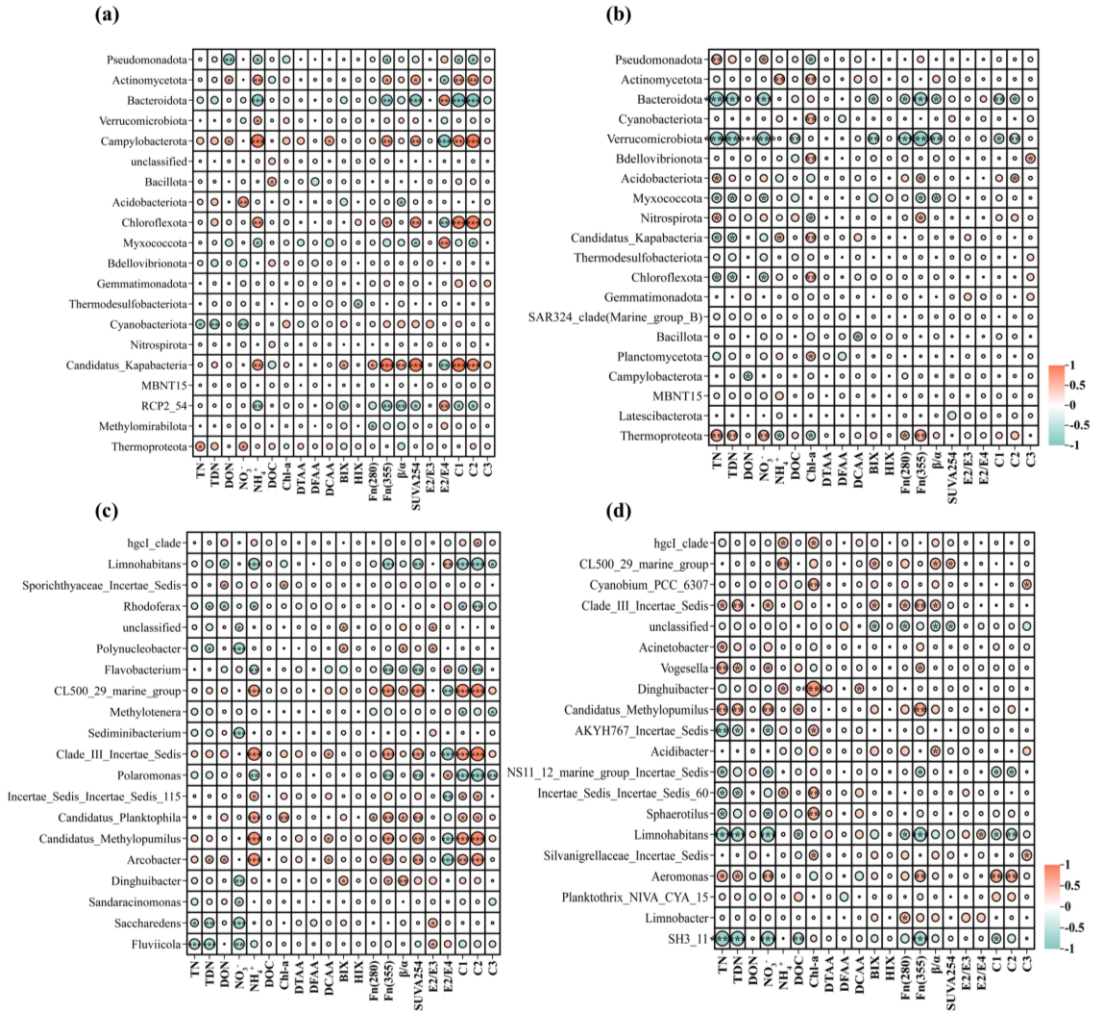

Fig. S10. Spearman correlation between nitrogen related parameters and bacterial relative abundance at (a-b) phylum level and (c-d) genus level during (a, c) dry and (b, d) wet season.

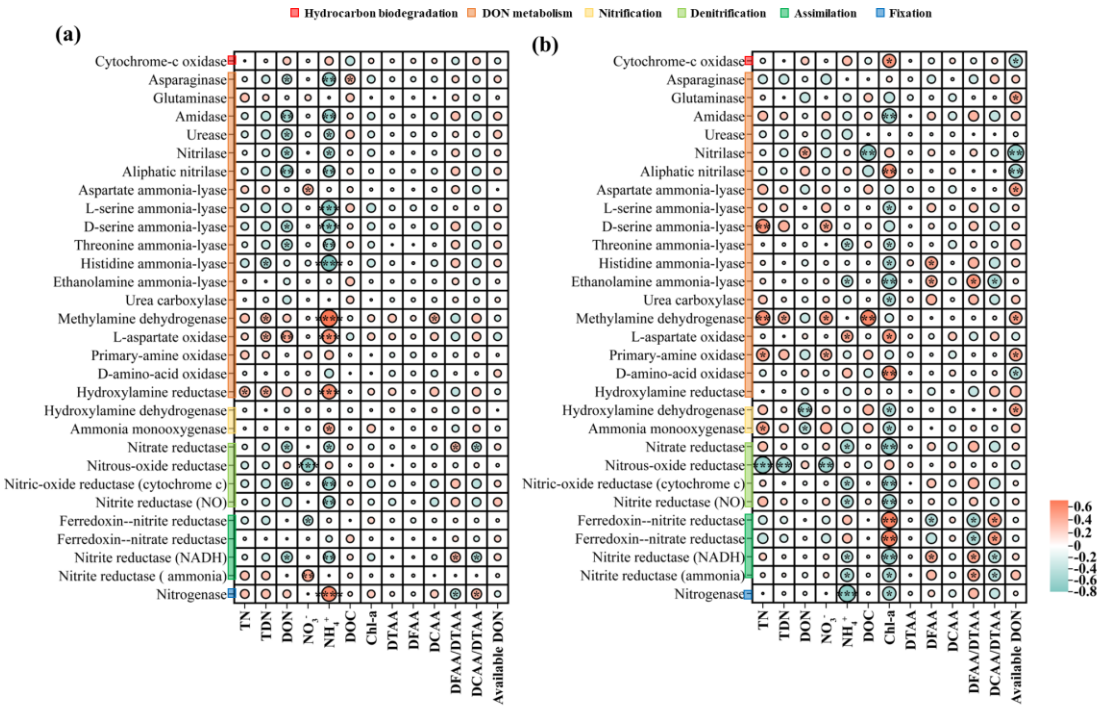

Fig. S11. Spearman correlation between nitrogen related parameters and PICRUSt-predicted bacterial N metabolism according to the genome (KEGG) enzyme profiles during (a) dry season and (b) wet season.

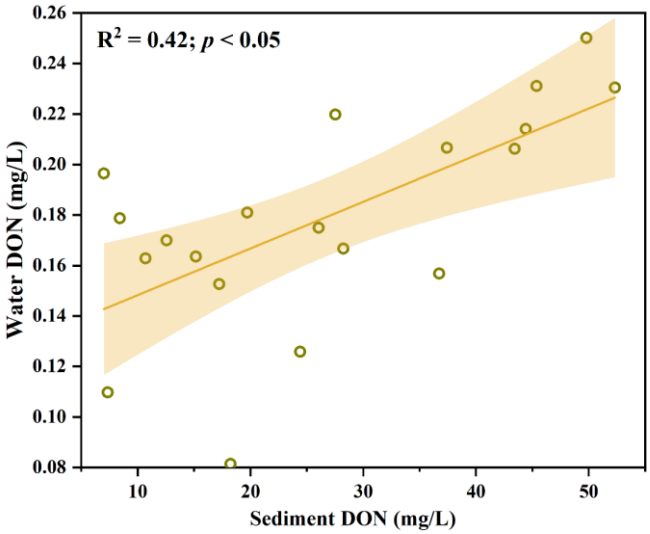

Fig. S12. The relationship between sediment and water DON concentrations during the dry season

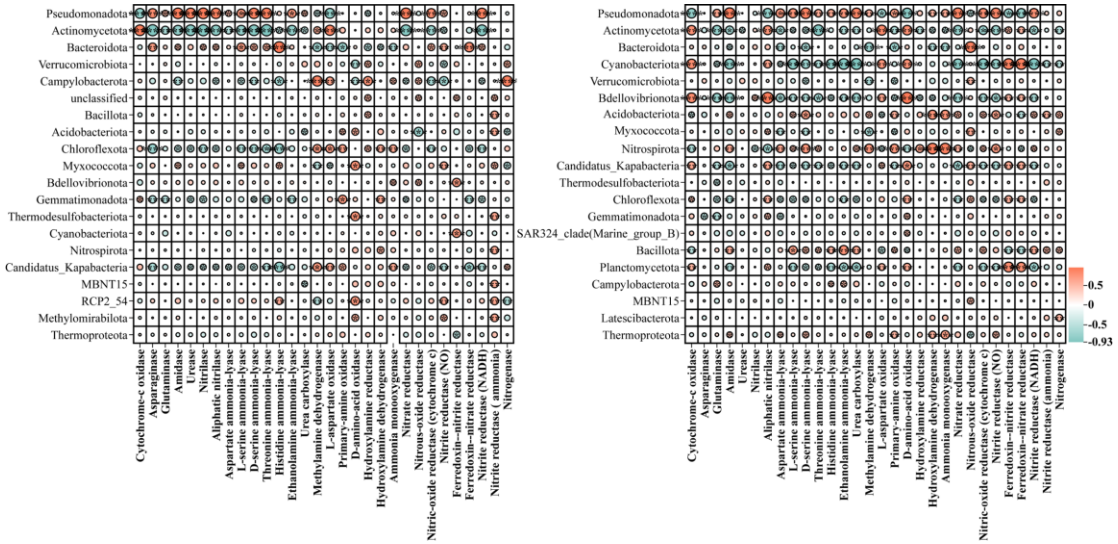

Fig. S13. Spearman correlation between phylum-level bacterial relative abundance and PICRUSt-predicted bacterial N metabolism (left) dry and (right) wet seasons.